International Journal of Fatigue 166 (2023) 107283

Contents lists available at ScienceDirect

International Journal of Fatigue

journal homepage: www.elsevier.com/locate/ijfatigue

Uniaxial and multiaxial fatigue behaviour of wire arc additively manufactured ER70S-6 low carbon steel components

Anna Ermakova [a], Javad Razavi [b], Filippo Berto [b], Ali Mehmanparast [a,*]

[a] Department of Naval Architecture, Ocean and Marine Engineering, University of Strathclyde, Glasgow G1 1XQ, United Kingdom
[b] Norwegian University of Science and Technology (NTNU), Trondheim, Norway

A B S T R A C T

Wire arc additive manufacturing (WAAM), also known as directed energy deposition (DED) process, is an efficient additive manufacturing technology, offers high potential to rapidly fabricate large-scale parts with complex geometries layer-by-layer. However, the fundamental understanding of the fatigue behaviour of such parts and the material requirements need to be significantly improved at all levels before this unique technology can be implemented for critical applications. This work aims to investigate the fatigue behaviour of WAAM built ER70S-6 steel under uniaxial, torsion and multiaxial loading conditions. Specimens were extracted in two different orientations: vertical and horizontal, to explore if the orientation direction has any effect on the fatigue results. Scanning Electron Microscopy (SEM) was conducted to examine the fracture surface of broken specimens and identify crack initiation regions and fracture mechanisms. The obtained results were compared with the fatigue data available in the literature on common structural steels fabricated using conventional welding and WAAM technique, showing similar fatigue behaviour with wrought S355 specimens. Moreover, the uniaxial data set on ER70S-6 WAAM specimens was evaluated according to the DNV RP-C203 standard for continuous welds, demonstrating advantageous fatigue resistance in the examined material.

1. Introduction

Additive manufacturing (AM) is a process of joining material layer by layer to produce objects from a three-dimensional model, using a combination of the energy source and material deposition. This manufacturing process offers some advantages compared to the conventional production techniques; for instance, more design freedom, material waste reduction, shorter lead-time, near net shape fabrication without expensive production moulds and tools. On the other hand, AM parts may contain defects related to the welding manufacturing process (lack of fusion, trapped gas bubbles, etc) [1], locked in residual stresses and rough surfaces [2]. Moreover, due to repeating heating and cooling processes during production, the material can experience different thermal histories and hence different microstructures, resulting in highly anisotropic behaviour which would subsequently affect the fatigue strength, wear, and corrosion resistance [3–5].

Development of more powerful and economical manufacturing processes enables the rapid production of larger components using common engineering materials, such as structural steels, for various industrial applications [6]. Wire arc additive manufacturing (WAAM) technique is a type of the directed energy deposition (DED) AM process, which meets the requirements for the large-scale component production offering the highest deposition rates among all AM methods: 5–8 kg/h compared with 55 g/h for the powder-based techniques [7]. With comparatively easy deposition process completed in open air, WAAM can be used for alternative re-manufacturing and repair applications in various industries such as offshore structures operating in remote areas [8].

It has been estimated that fatigue contributes to approximately 90% of all mechanical service failures; therefore, fatigue analysis is an essential part of any structural design assessment and inspection planning, especially for AM built components, in which welding defects and tensile residual stresses are detrimental for fatigue characteristics [9]. Thus, for future structural applications the uncertainty of the fatigue performance of AM components must be fully characterised and new test data need to be generated for structural durability predictions. Due to the increasing interest by aerospace and nuclear industries in AM technologies, a significant majority of the existing experimental fatigue data in the literature are available on AM built titanium Ti-6Al-4 V specimens [2,10–14] and stainless steel SS316 [15,16]; however, only a limited number of the available data sets are on fatigue behaviour of WAAM built steels for application in other industries, such as offshore renewable energy in which the structures are commonly made of structural steels. Among the limited data available on WAAM built steels in the literature, a study was carried out by Dirisu et al. [17] on the fatigue performance of ER70S-6 alloy. Flat dog bone specimens were extracted from the WAAM walls in horizontal orientation (i.e. parallel to

* Corresponding author.
E-mail address: ali.mehmanparast@strath.ac.uk (A. Mehmanparast).

https://doi.org/10.1016/j.ijfatigue.2022.107283
Received 18 July 2022; Received in revised form 8 September 2022; Accepted 16 September 2022
Available online 21 September 2022

Nomenclature

A	material dependent constant
B	material dependent constant
k	inverse slope in S-N curve
N_f	number of cycles to failure
R	load ratio
T_σ	Scatter index
λ	biaxiality ratio
$\Delta\sigma$	stress range
$\Delta\sigma_{50\%}$	fatigue strength at 2×10^6 cycles
σ_{eff}	effective stress
σ_{max}	maximum stress
Φ	phase angle
AM	Additive Manufacturing
CMT	Cold Metal Transfer
DED	Directed Energy Deposition
EDM	Electrical Discharge Machining
H	Horizontal
SB	Smooth round bars
SEM	Scanning Electron Microscope
V	Vertical
WAAM	Wire Arc Additive Manufacturing

the deposition direction) and three specimen types were examined: as-built, as-built rolled and machined. All specimens were tested under uniaxial fatigue loading condition with the load ratio of $R = 0.1$. The test results demonstrated an improvement in the fatigue strength for the machined specimens with smooth surface compared to other specimen types. It has been also reported that rolling of the as-built wavy surfaces was found beneficial to enhance the fatigue performance of the WAAM built components compared to as-built specimens. These findings confirmed that wall waviness, which is in fact naturally occurred notches during manufacturing process, acts as a stress riser and therefore reduces the fatigue strength of the as-built components. Another study was conducted by Bartsch et al. [6] on as-built WAAM G3Si1, a copper coated steel, specimens. Dog bone specimens with two different lengths were tested under uniaxial fatigue loading conditions with the load ratio of $R = 0.1$ The presented experimental and numerical results revealed that the surface roughness was the main influencing factor in fatigue life analysis of the examined specimens.

A review of the existing works available in the literature shows that only a few fatigue data sets were generated for WAAM built structural steels, which only included uniaxial fatigue loading conditions. The lack of wider range of fatigue data for WAAM built steel components restricts the industry's access to the full range of advantages that the WAAM technology offers to a wide range of industries and limits the implementation of this powerful technology into new manufacturing procedures. In this context, the current work aims to contribute to the fundamental understanding of the fatigue and cracking behaviour of additively manufactured ER70S-6 specimens subjected to uniaxial, torsion and multiaxial fatigue loading conditions. The experimental data obtained from this study was compared with the existing fatigue data for wrought structural steels and also with limited data available on WAAM built components. Also included in this study is the sensitivity analysis of the fatigue behaviour to the specimen extraction orientation (parallel or perpendicular) with respect to the deposition direction. Last yet importantly, the presented results from this study were interpreted by conducting complementary microscopic analysis of the fracture surfaces to better understand the failure mechanism under different type of fatigue loading conditions.

2. Specimen manufacturing process

For conducting fatigue tests in the present study, four WAAM walls were built using Lincoln Electric ER70S-6 welding wire [18], with the chemical composition summarised in Table 1. The Cold Metal Transfer (CMT) based WAAM process was implemented, with manufacturing process parameters summarised in Table 2. To minimise the microstructural variability of different WAAM walls, all manufacturing parameters were kept the same for all four walls. Each WAAM wall was built in the middle of the base plate, made of EN10025 rolled structural steel, with dimensions of approximately $420 \times 200 \times 12$ mm^3. As shown in Fig. 1, the base plate was rigidly fixed onto the working table using eight clamps (two on each side of the base plate). This helped to minimise bending and distortion of the base plate and WAAM wall due to high manufacturing temperatures. The clamps were released once the wall was completed and cooled down to the ambient temperature. Additive layers were deposited on top of each other using an oscillation pattern [8], in order to produce relatively thick walls of approximately 24 mm in thickness (Y-direction in Fig. 1), 355 mm in length (X-direction) and 140 mm in height (Z-direction). As shown in Fig. 1, the WAAM fabrication set-up consisted of the CMT power source, a robotic arm with the torch feeding the wire and supplying shielding gas simultaneously. An exhaust fan was set above the WAAM wall to remove the generated heat and fumes.

Upon completion of the WAAM walls fabrication process, sixty smooth round bar (SB) specimens were extracted using the Electrical Discharged Machining (EDM) technique. Specimens were extracted along two different orientations: vertical (V) – perpendicular to the AM layers, and horizontal (H) – oriented along the deposited layers. An example of the schematic extraction plan for one of the WAAM walls is displayed in Fig. 2 (a), where specimens denoted B-1 – B-6 have horizontal and B-7 – B-16 have vertical orientations. The round bar specimens were designed in accordance with the ASTM E466 standard [19], and the key dimensions are presented in Fig. 2 (b).

3. Testing and data analysis methodology

3.1. Fatigue tests

All fatigue tests under uniaxial, torsion, and multiaxial loading

Table 2
CMT-WAAM fabrication process parameters.

Shielding gas	Ar + 20% CO_2
Gas flow rate	15 L/min
Wire diameter	1.2 mm
Robot travelling speed	7.33 mm/sec
Wire feed speed	7.5 m/min
Dwell time	120 sec

Table 1
Chemical composition of ER70S-6 material (wt.-%)[18].

	C	*Mn*	*Cr*	*Si*	*Ni*	*Mo*	*S*	*P*	*Cu*	*V*
ER70S-6	0.09	less than1.60	0.05	0.09	0.05	0.05	0.007	0.007	0.20	0.05

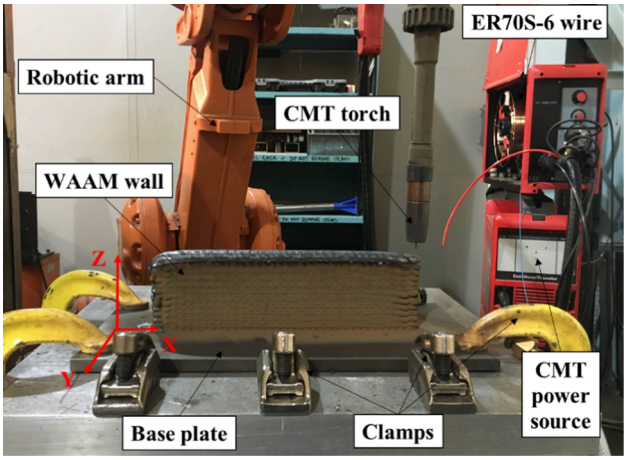

Fig. 1. CMT system set up and the WAAM deposition process.

conditions were performed using an MTS landmark servo-hydraulic test machine with the load cell capacity of 100 kN, under load control mode with a frequency of 20 Hz and the load ratio of $R = 0.01$. The test machine was accurately tuned prior to the start of the testing phase to ensure that the intended load levels were precisely applied on the test specimens. Moreover, alignment checks were conducted to ensure that the fatigue response of the WAAM built material is examined in the absence of any bending stresses. For multiaxial fatigue tests, a biaxiality ratio of $\lambda = 1$ was used, with phase angle $\Phi = 0^0$ (in phase loading). The stress-fatigue life diagrams were obtained separately for vertical and horizontal specimens, to capture the sensitivity of the fatigue behaviour to specimen extraction orientation. On average around 10 specimens were tested for each fatigue loading condition (uniaxial, torsion and multiaxial) and specimen orientation (vertical and horizontal). In this experimental test programme, specimens that endured 2×10^6 cycles were considered as run-out. The obtained fatigue data were analysed using 10% (upper bound), 50% (mean curve) and 90% (lower bound) probability of failure bands according to procedure described in the BS ISO 12107:2003 [20] and ASTM E739-10 [21] standards, and the data were plotted to obtain the inverse slope, k, of the Wöhler curves and scatter index, T_σ, in the fatigue data analysis. In this assessment, T_σ is the ratio between the stress level corresponding to 10% and 90% of survival probability. The calculated stresses for uniaxial loading were the nominal stress at the net section of the specimen. In case of torsion loading, the presented stresses were the maximum values in the cross section (the stress at the surface). As for the multiaxial loading, since the biaxiality ratio was $\lambda = 1$, only one of the stresses (tension or torsion) was used for illustration.

According to the procedure given in the literature, the uniaxial fatigue data can be analysed using the following equation, which is often referred to as Basquin relationship.

$$N_f = A(\Delta\sigma)^B \tag{1}$$

Equation (1) shows that the number of cycles to failure N_f can be correlated with the cyclic stress range $\Delta\sigma$ using a power-law equation. The power-law constants in this equation, A and B, are material dependent and can be obtained using a line of best fit made to the data. In this research, a similar approach has been adopted by plotting the maximum applied stress against the number of cycles to failure in uniaxial fatigue tests. The inverse slope obtained from this analysis is: $k = 1/B$. Similar power-law relationships have been employed to correlate torsion and multiaxial fatigue stresses with the number of cycles to failure.

3.2. Fractography analysis

Upon completion of the fatigue tests, six specimens were selected for post-mortem microscopy analysis to study the failure mechanisms in the specimens subjected to different type of fatigue load (uniaxial, torsion and multiaxial) and oriented along different directions (vertical and horizontal). The fractography analysis was carried out using the FEI Quanta 650 FEG scanning electron microscope (SEM). In order to directly compare the observations on the fracture surfaces, the specimens subjected to the same fatigue load level with different orientations and fatigue load types were selected for the SEM analysis. The results obtained from the post-mortem analysis were implemented in conjunction with the experimental data in order to provide an accurate interpretation of the fatigue behaviour of the WAAM built specimens under different fatigue load types and for different specimen orientations.

4. Experimental results and discussions

4.1. Fatigue test results

The fatigue test data for WAAM built ER70S-6 specimens for different specimen orientations and different loading types are shown in Fig. 3 in log–log axes. These data were analysed following the procedure detailed in Section 3.1, by plotting the maximum stress against the number of cycles to failure, and the resulting fatigue properties are summarised in Table 3. In this table, $\Delta\sigma_{50\%}$ is the fatigue strength at 2×10^6 cycles, T_σ is the scatter index, and k is the inverse slope factor. The experimental data from uniaxial fatigue tests on vertical and horizontal specimens are presented in Fig. 3 (a) and (b), respectively, with the obtained trends directly compared with each other in Fig. 3 (c). It can be observed in Fig. 3 (a–c) that under uniaxial loading condition the fatigue strength of 436 MPa and 384 MPa was obtained for vertical and horizontal specimens, respectively, indicating that the fatigue strength of the vertical specimens was higher than the horizontal. Comparison of the S-N data sets for different specimens orientations in Fig. 3 (c) shows that a much steeper slope can be observed for the horizontal specimens, which

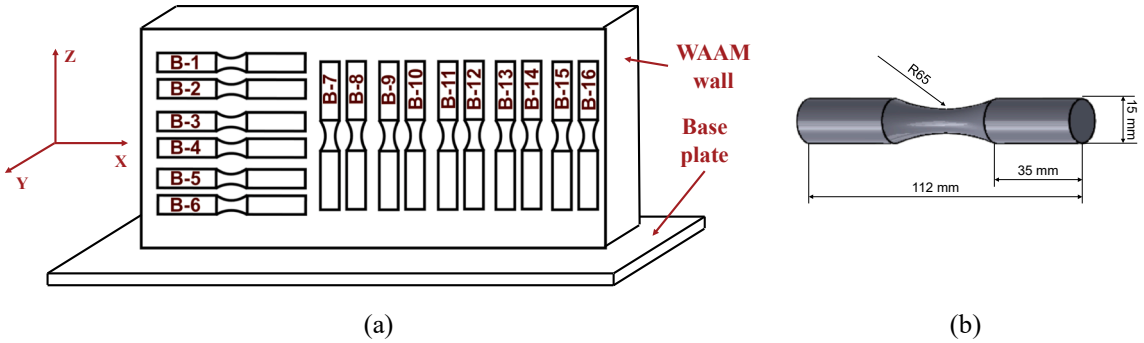

Fig. 2. (a) Schematic extraction plan for a WAAM wall, and (b) cylindrical specimen dimensions.

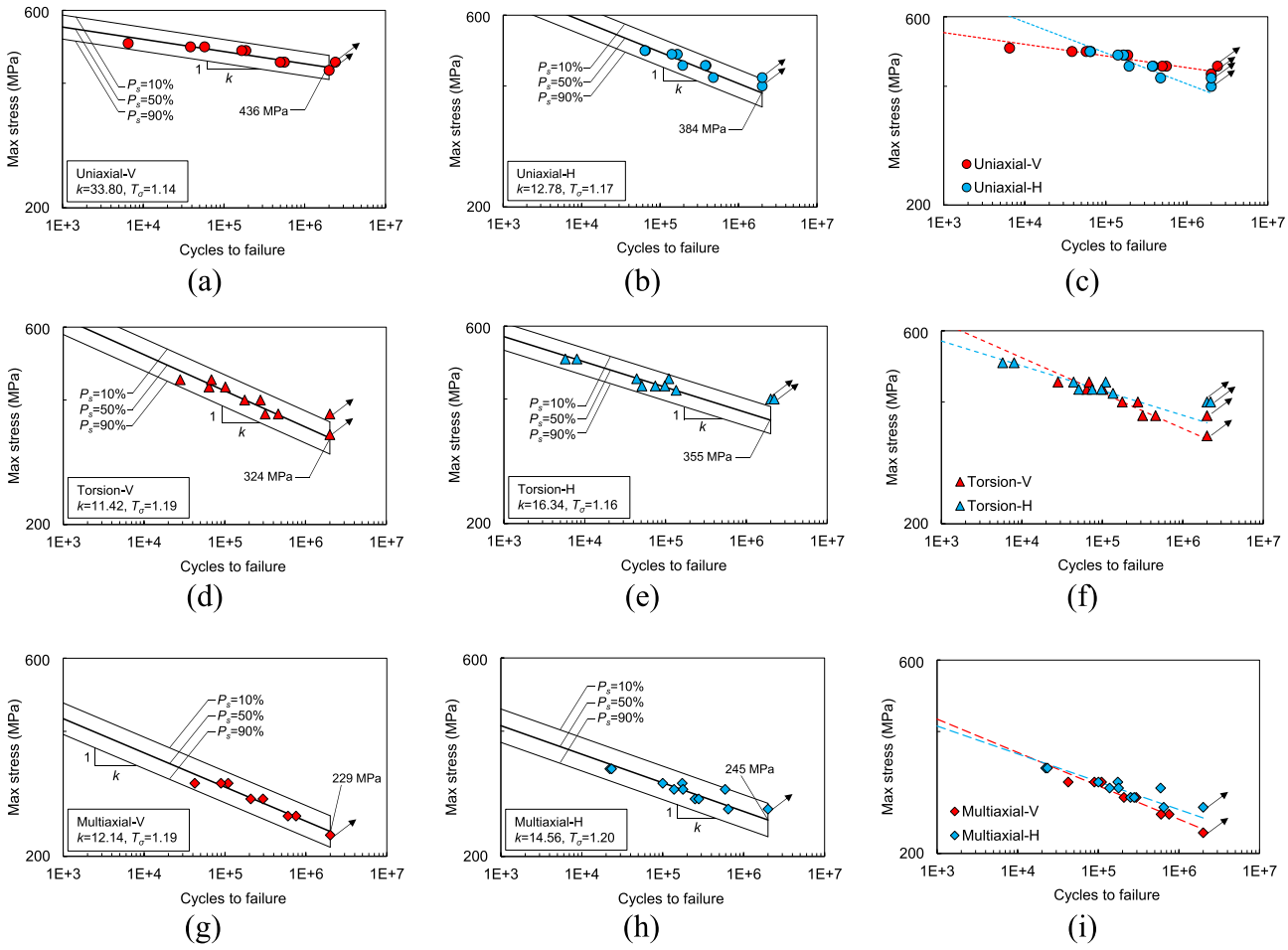

Fig. 3. Fatigue test data for ER70S-6 specimens under (a-c) uniaxial, (d-f) torsion, and (g-i) multiaxial loading conditions.

Table 3
Fatigue behaviour of tested ER70S-6 specimens.

Test	Orientation	$\Delta\sigma_{50\%}$ [MPa]	T_σ	k
Uniaxial	V	436	1.14	33.80
	H	384	1.17	12.78
Torsion	V	324	1.19	11.42
	H	355	1.16	16.34
Multiaxial	V	229	1.19	12.14
	H	245	1.20	14.56

is also indicated by the inverse slope factor that is 2.6 times higher for the vertically oriented specimens compared to the horizontal samples reported in Table 3. As it was previously reported by Ermakova et al. [22], WAAM built ER70S-6 specimens with horizontal orientation have a higher yield strength (390 MPa) than the vertical (365 MPa), hence it is expected that the material with higher yield strength (horizontal orientation) will have a lower fatigue life [23], confirming the trends observed in Fig. 3 (a–c). Moreover, having higher value of yield strength along with higher elongation at failure (higher ductility), possibly resulting in higher fatigue strength at high load level for horizontal specimens (0.77 mm/mm), compared with the vertical (0.71 mm/mm) [22]. It also can be noted here that the fatigue strengths obtained in the study for the horizontal and vertical specimens are close to and above the orientation-specific yield stress of the material, respectively. As seen in Table 3 the analysis of the test results show that the scatter index observed in uniaxial fatigue data is comparable for both specimen orientations and differs only by 2%. Finally observed in the uniaxial fatigue data is that while the fatigue life in horizontal specimens is generally lower than the vertical specimens at low stress levels, this trend can be switched at higher stress levels if the obtained trend from horizontal specimens is extrapolated to the high stress region.

The fatigue data from torsion tests on vertical and horizontal specimens are presented in Fig. 3 (d) and (e), respectively, with the obtained trends directly compared with each other in Fig. 3 (f). As seen in Fig. 3 (d-f), the fatigue strengths of vertical and horizontal specimens are found to be 324 MPa and 355 MPa, respectively, indicating similar, though slightly higher, fatigue strength in horizontal specimens compared to the vertical. This increase in the fatigue strength of horizontal specimens tested under torsion can be attributed to the higher ductility of this orientation resulting in higher stress shielding in the specimen. As seen in Table 3 the analysis of the torsion test results show that the scatter index is similar for both orientations with 1.19 for vertical against 1.16 for horizontal specimens. Moreover, the inverse slope factor has been found to be higher for horizontally oriented specimens compared to vertical by 43%, with a steeper slope for the vertical specimens data set.

The fatigue data from multiaxial fatigue tests on vertical and horizontal specimens are presented in Fig. 3 (g) and (h), respectively, with the obtained trends directly compared with each other in Fig. 3 (i). It can be observed in Fig. 3 (g) and (h) that the fatigue strengths obtained from vertical and horizontal specimens under multiaxial loading condition are 229 MPa and 245 MPa, respectively, indicating 6.5% higher value of fatigue strength for the horizontal specimens compared to the vertical. Analysing the experimental data from multiaxial tests shows that the values for the scatter index in vertical and horizontal data sets are comparable within 0.8% for specimens with different orientations. Finally observed in the results from multiaxial fatigue test data is that

the difference in the inverse slope factors for specimens with different orientations drops to 16.6%, with slightly higher value (hence lower slope) observed for the horizontal specimens compared to the vertical data set (see Table 3). It should be noted here that the presented preliminary trends in this study are indicative representation of the fatigue behaviour of WAAM built ER70S-6 specimens, hence further repeat tests need to be performed in future work to produce the S-N design curve for this material and provide higher confidence in the statistical analysis by considering the inherent scatter in the data for industrial applications.

Further comparison of all fatigue data obtained from the current study is presented in Fig. 4. This figure shows that a decreasing overall trend in fatigue strength can be observed from uniaxial fatigue to torsion and further to multiaxial fatigue tests. The analysis of the presented results in Fig. 4 and Table 3 reveals that compared to the uniaxial test results the average fatigue strength of the material (i.e. the mean value between fatigue strength of vertical and horizontal specimens) drops by 15% for specimens tested under torsion and by 42% for specimens tested under multiaxial loading condition considering solely the tension or torsion applied stress. This observation confirms that the fatigue strength of the ER70S-6 WAAM built specimens is sensitive to the fatigue loading type, as expected. Moreover, the experimental data obtained from specimens with different orientations indicates that in addition to the type of the fatigue loading (i.e. uniaxial, torsion and multiaxial), the results are also sensitive to the specimen orientation. Comparison of the fatigue strengths in vertical and horizontal specimens tested under different fatigue loading types shows that highest difference, which is 12%, is observed in specimens tested under pure uniaxial loading condition, whereas this difference gradually reduces to 9% in torsion fatigue tests and 6.5% in multiaxial fatigue tests. It is also worth noting that due to varying inverse slope factors for data sets with different specimen orientations obtained under different fatigue load types, the data sets intersect when the observed trends are extrapolated to lower number of cycles. This suggests that the performance of one specimen orientation is better at lower number of cycles and then gradually deteriorates at higher number of cycles, and vice versa. The general observation in Fig. 4 shows that under torsion and multiaxial loads, horizontal specimens display higher fatigue strengths at 2 million cycles (run-out limit) than vertical, whereas for uniaxial load, the vertical orientation exhibits a higher fatigue strength than the horizontal.

4.2. Comparison with the literate data and design curves

In order to assess the fatigue performance of ER70S-6 WAAM built specimens for fatigue design and life assessment of offshore structures, the obtained fatigue data from this study have been compared with the S-N fatigue design curve recommended for the continuous welds (C1) by the DNV RP-C203 standard [24], and with available data in the literature on uniaxial, torsion and multiaxial fatigue for structural steels. It is known that the fatigue behaviour of engineering materials is dependent on the load ratio and specimen design [25,26]; however, due to the limited data available in the literature some of the data presented in this section are for specimen designs that differ from the ones employed in this study. In order to normalise the fatigue data under various stress ratios collected form the literature into a single fatigue plot, the effective stress model was employed, using the following Equation (2). The concept of the effective stress was introduced by Li et al.[27] and is used for direct comparison of fatigue data from different studies. This model does not consider the effect of loading frequency, therefore limited effect of different loading frequencies is expected.

$$\sigma_{eff} = \sigma_{max}\left(\frac{1-R}{2}\right)^{0.28} \quad (2)$$

It can be seen in Fig. 5 that the obtained experimental data for ER70S-6 WAAM built specimens from this study fall ahead of the C1 design curve from the DNV standard for horizontal specimens above 10,000 cycles, and for vertical specimens above 39,500 cycles, indicating that with the exception of extremely high stress range values the DNV recommended C1 design curve provides a conservative estimate of the fatigue life in ER70S-6 WAAM built specimens. Having said that, it can be seen that the slopes for the experimental S-N curves are lower compared with the standard curve.

Along with the C1 S-N fatigue design curve provided by DNV standard, the 50% uniaxial fatigue failure bands (i.e. mean curves) for ER70S-6 WAAM built specimens were also compared with a series of S-N curves obtained from S355 wrought steel specimens. S355 structural steel is commonly used in offshore structure and marine renewable energy applications, hence the results were compared with this material to assess the suitability of WAAM built steel structure for offshore applications [28,29]. Large dog bone S355 specimens tested at $R = 0.1$ by Anandavijayan et al.[23], smaller flat dog bone specimens assessed at $R = -1$ by Corigliano et al.[30], cylindrical specimens tested at $R = 0.01$ by Dantas et al.[31], and at $R = -1$ by Aeran et al.[32], fillet welded cruciform specimens examined at $R = 0$ by Berto et al.[33], and S-N curves for wrought C40 carbon steel cylindrical specimens generated at $R = -1$ by Atzori et al.[34] were considered for comparison with the results obtained from the present study. Moreover, the uniaxial fatigue data available on ER70S-6 WAAM built flat dog bone specimens tested at $R = 0.1$ by Dirisu et al.[17] and G3Si1 WAAM as built flat dog bone specimens (with rough surface) tested at $R = 0.1$ for two different specimen designs by Bartsch et al.[6] were used for comparison purposes. All experimental uniaxial data from the literature are summarised and presented in Fig. 6 (a) as effective stress versus number of cycles.

Comparison of the obtained data from the present study with the S-N curves literature data on S355 steel specimens reveals that the uniaxial data for ER70S-6 WAAM built specimens overlap with the upper bound for the S355 cloud, suggesting generally higher fatigue life compared to the wrought material. The direct comparison with the results on S355

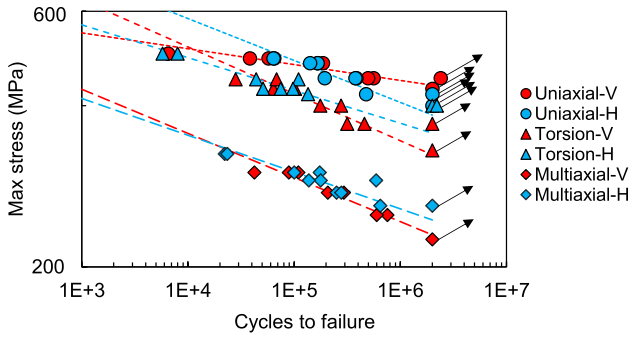

Fig. 4. Comparison of all experimental data for ER70S-6 WAAM specimens under different fatigue load types.

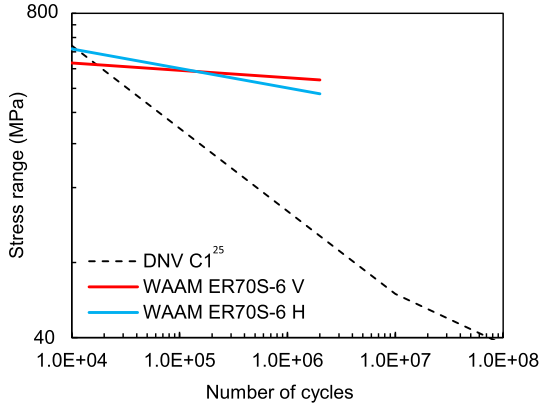

Fig. 5. Comparison of uniaxial fatigue data for ER70S-6 WAAM specimens with the DNV C1 standard.

specimens with similar design and tested with the same stress ratio $R = 0.01$ [31] demonstrates that the higher fatigue life was exhibited in WAAM specimens, where S355 S-N curve has similar slope with the vertical WAAM specimens. It can be seen in Fig. 6 (a) that a different specimen design from an independent study on ER70S-6 WAAM specimens tested under different loading conditions [17] resulted in S-N curve slightly below the horizontal and vertical curves obtained from this study, confirming the general trend for the WAAM specimens made with ER70S-6 steel and highlighting the sensitivity to the test frequency and specimen design. The above observations lead to a conclusion that ER70S-6 steel parts produced by means of WAAM technology can be considered for manufacturing or repair of offshore structures and an alternative to conventional structural steels and manufacturing technologies.

Due to the limited data available on torsion and multiaxial fatigue for steels in the literature, only a few curves were found and presented for comparison with the experimental data from this study in Fig. 6 (b) and (c), data is also presented as effective stress versus number of cycles. One source presents the behaviour of cylindrical C40 carbon steel specimens tested with loading ratio of $R = -1$ for torsion and $R = 0$ for multiaxial tests by Atzori et al.[34], and another source covers cylindrical 39NiCrMo3 steel specimens examined under $R = -1$ by Berto et al.[35] Additional data set was found and displayed for multiaxial fatigue comparison on wrought cylindrical S355 specimens tested under $R = 0.01$[31], hence valid for the direct comparison with the data obtained from the present study. For presented multiaxial fatigue data a biaxiality ratio was $\lambda = 1$, with in phase loading angle $\Phi = 0^0$. It can be seen in Fig. 6 (b) that the torsion fatigue trends for WAAM ER70S-6 specimens fall close to the 39NiCrMo3 steel specimens, and above C40 carbon steel. With regards to multiaxial fatigue behaviour, the results for WAAM tested specimens in Fig. 6 (c) are above those obtained for C40 carbon steel specimens with shallower slope, but lower than S355 and 39NiCrMo3 steel. The slope for S355 specimens is similar to the data obtained from this study, and the data set falls slightly above the ER70S-6 WAAM built specimens data, suggesting similar but slightly higher fatigue life under multiaxial loading in S355 specimens.

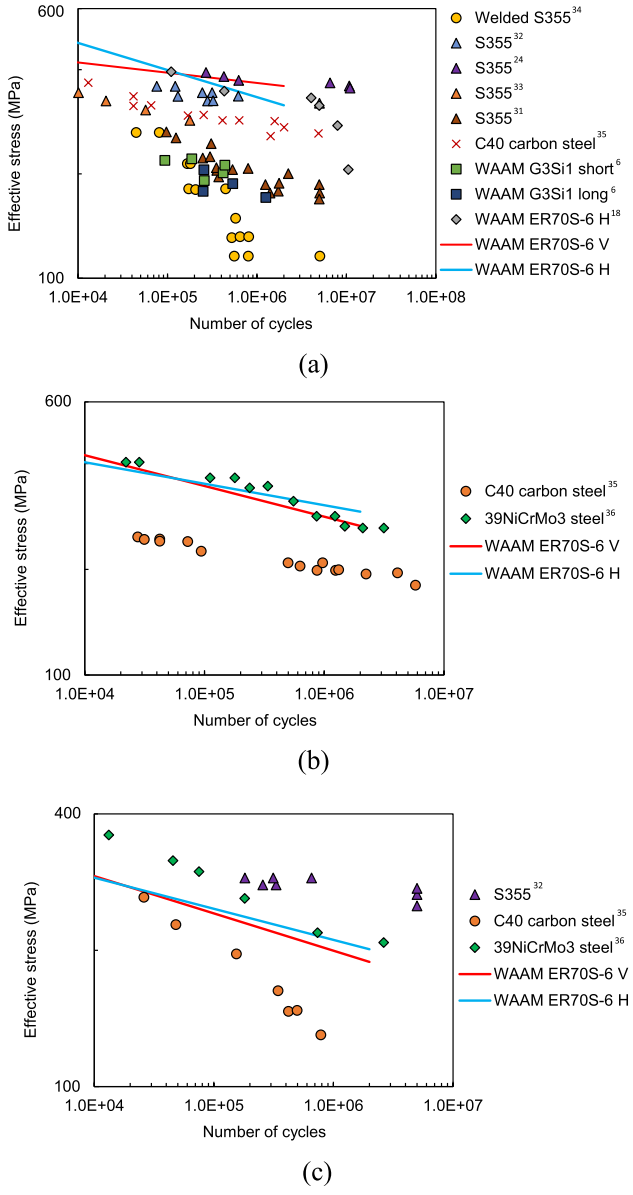

Fig. 6. Comparison of the obtained fatigue data from ER70S-6 WAAM specimens with the literature data on: (a) uniaxial, (b) torsion and (c) multiaxial fatigue tests.

4.3. Fractography analysis

The microstructural investigation by means of SEM showed an almost defect-free material in all ER70S-6 WAAM built specimens with some occasional defects with dimensions of less than 30 μm. The fractography analysis was performed on fatigue tested specimens to examine differences in failure mechanisms in specimens with different orientations under different types of fatigue loading condition (uniaxial, torsion and multiaxial). Examples of fracture surfaces obtained from uniaxial fatigue tests under 480 MPa are shown in Fig. 7 (a) for vertical and Fig. 7 (b) for horizontal ER70S-6 WAAM built specimens. Four distinct crack growth stages are indicated in both figures, starting with the crack initiation in area 1, crack growth in area 2 (where white arrows show the direction of the crack growth propagation), and ductile failure in region 3 due to unstable fatigue crack growth, followed by the ductile failure in region 4 due to fast fracture. The presented fracture surface for the horizontal specimen consists of two crack initiation sites (Fig. 7 (b)), in which cracks started simultaneously in two parallel planes and subsequently merged into one in the crack growth area 2. In both cases the crack nucleated from the surface irregularities. In the crack growth region for both vertical and horizontal specimens the fatigue striations can be observed, which are perpendicular to the crack growth plane (marked with yellow arrows). Also observed in the figures are the elongated fracture features parallel to the crack growth direction (shown in yellow dashed lines). The fracture surface in regions 1 and 2 for the vertical specimens indicates shallower ductile features, whereas the fracture surface of horizontal specimen in the same regions exhibits deeper dimples. This is in good agreement with slightly higher ductility of the horizontal specimens. Lastly, it can be observed that even though both specimens were tested under the same loading condition uniaxial fatigue load, the areas for first three crack growth stages 1–3 are larger for the vertical specimen, which resulted in longer performance of the specimen under this load level. The shorter fatigue life of the horizontal specimen in this case can also be affected by two independent crack planes contributing to the final failure of the specimen.

The failure surfaces of vertical and horizontal specimens tested under 448 MPa torsion fatigue load are shown in Fig. 8 (a) and (b), respectively. It can be seen in this figure that the outer diameter of the fracture surface is flat in both specimens, suggesting the contact of the two faces of initiated crack under mode III loading condition in these test specimens. The larger area of fracture surface in both cases indicates the evidence of abrasion, demolishing all fracture features under out-of-plane shear, by rubbing the fracture surfaces against each other. Only 18% of the fracture surface of vertical specimen and 28.5% of horizontal specimens retained fatigue fracture features. This was also reflected in exhibited number of cycles, which is 1.6 times higher for the vertical specimen compared to the horizontal specimen. The remaining fatigue

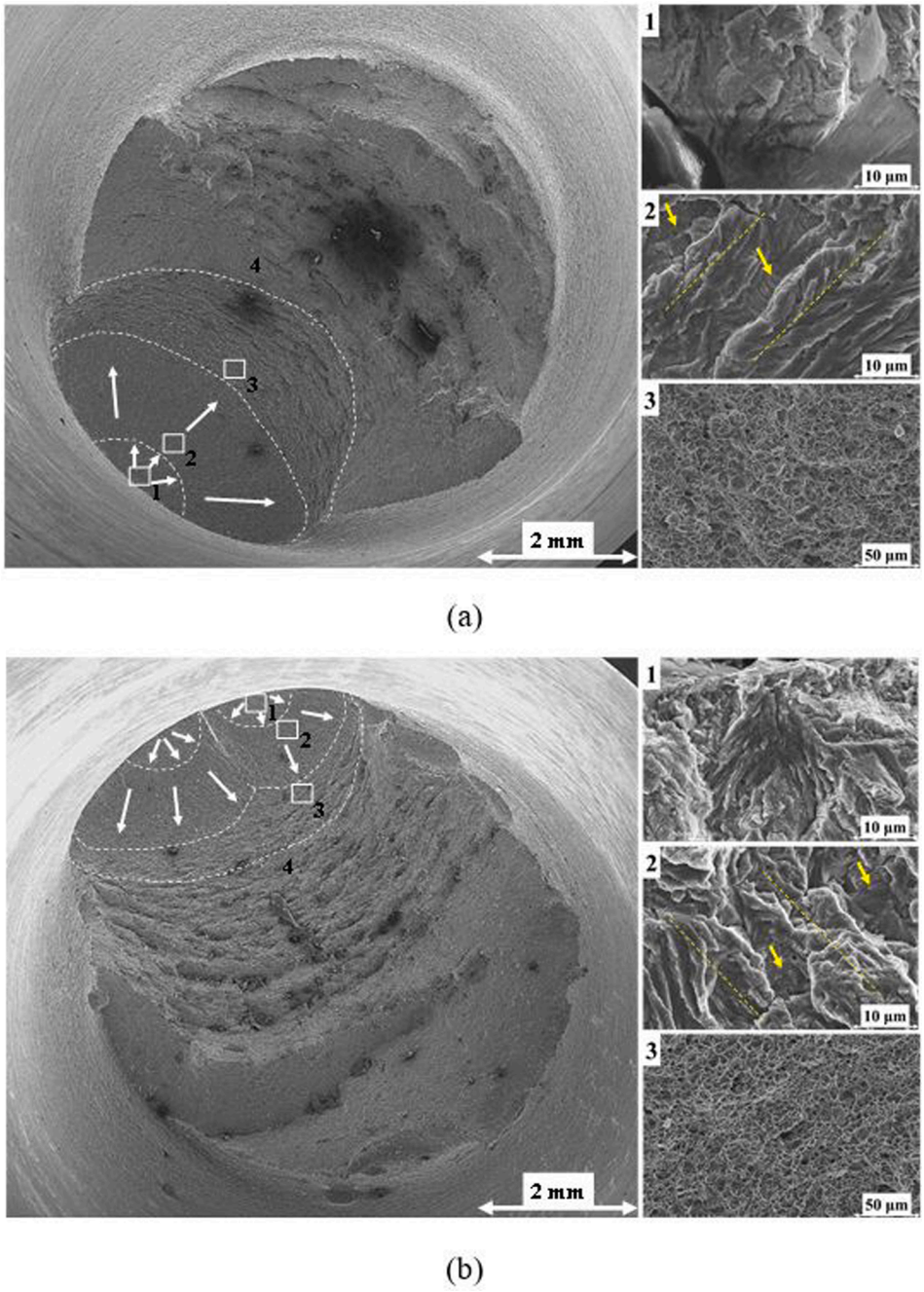

Fig. 7. Fracture surface of ER70S-6 WAAM built specimens tested under uniaxial loading condition (a) for vertical, and (b) for horizontal specimens, presenting crack initiation region (1), crack propagation region (2), and ductile fracture region (3), and fast fracture region (4).

fracture area is due to the final specimen failure under mode I fracture mechanics condition, resulting in cascade of several fatigue fracture planes with visible boundaries of ductile fracture between them (marked with white arrows), which is also referred to as 'factory roof' morphology[35,36]. The ductile cup and cone features are more pronounced for horizontally oriented specimen, which failed at lower number of cycles. Fatigue striations can be observed on the fracture surface of both specimens and highlighted with yellow arrows. Although the abrasion of crack planes eliminated some of the fracture features under torsion loading, by comparing fracture surfaces of the specimens tested under uniaxial and torsion fatigue it can be seen that the surface area after uniaxial testing is approximately two times smaller, due to ductile elongation of the specimen under pure mode I fracture mechanics condition.

Fracture surfaces of the specimens tested under multiaxial fatigue load of 300 MPa are shown in Fig. 9 (a) for vertical and (b) for horizontal specimens. Comparable features of 'factory roof' can be observed on both specimen surfaces, which are located in central part of the fracture area and indicated as region A. Similar to the fracture surfaces after torsion fatigue failure a considerable proportion (40–45%) of the two broken specimens has been found to be flat and consists of evidence of wear and abrasion, suggesting mode III fracture mechanics condition in region B. In this area two main fatigue features were observed and marked with yellow arrows: 1 – fatigue striations, and 2 – colonies of flat 'fish-bone' features indicating large striations near the specimen surface and parallel to it. The remaining cone surface is corresponding to the fast fracture which is shown as region C. As expected, due to combination of tension and torsion loading conditions the fracture surface area after

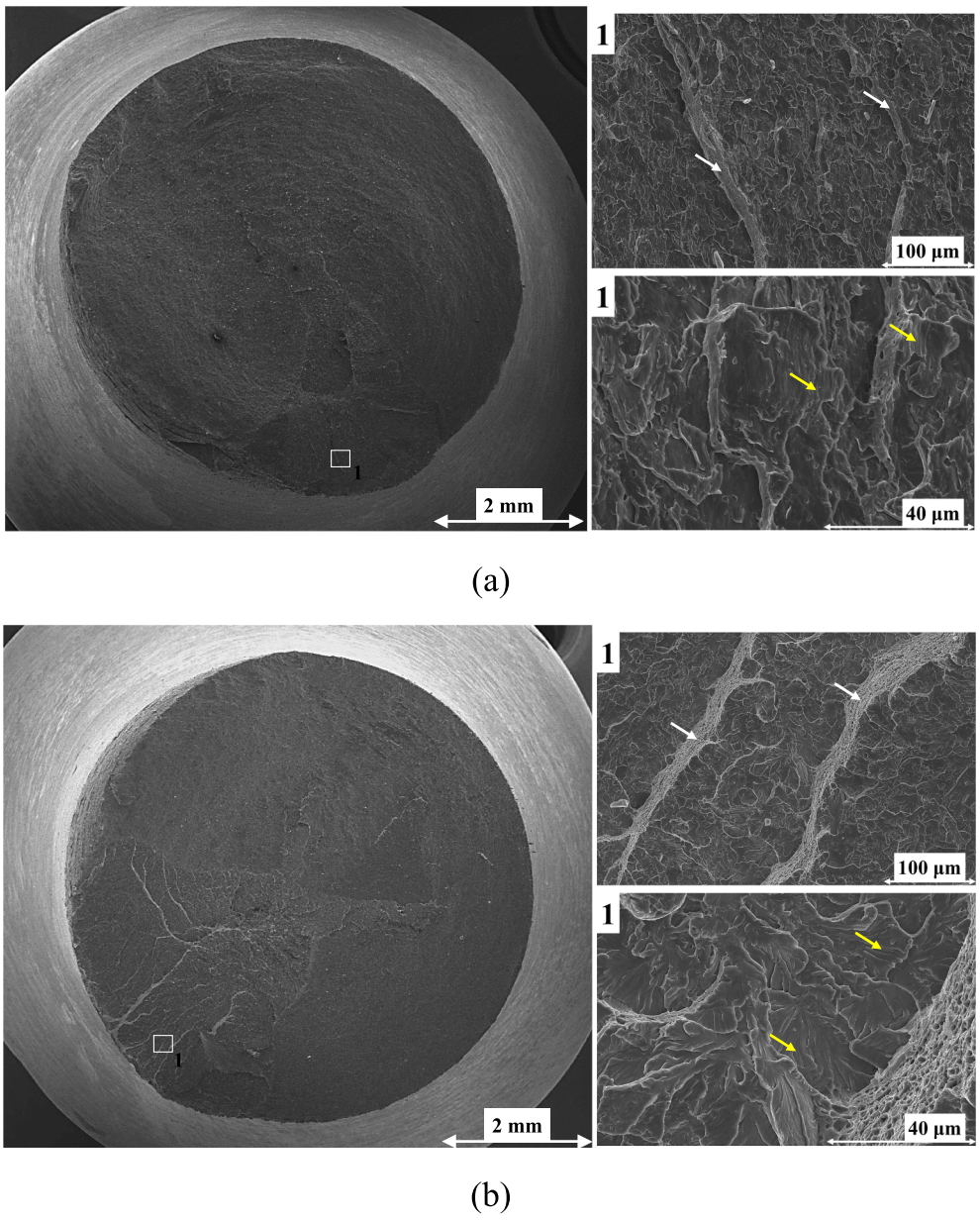

Fig. 8. Fracture surface of ER70S-6 WAAM built specimens tested under torsion loading condition (a) for vertical, and (b) for horizontal specimens.

multiaxial fatigue testing is larger than for pure uniaxial load (on average by 35%) and smaller than for pure torsion load (on average by 23%).

5. Conclusions

Fatigue tests were conducted on sixty ER70S-6 WAAM built specimens to examine the uniaxial, torsion and multiaxial fatigue properties. Specimens were extracted from the WAAM walls in two distinct orientations: vertical and horizontal. The main conclusions and observations from this study are summarised below:

- Sensitivity of the fatigue results to the specimen orientation was observed during this study. Higher fatigue strength was found for vertical specimens tested under uniaxial load, however, under torsion and multiaxial load, the horizontal specimens exhibited higher fatigue strength.
- The difference between fatigue strength for specimens with different orientations dropped for results obtained from torsion fatigue tests and further reduced for multiaxial fatigue compared with uniaxial test results.
- The S-N data show that material with the higher yield stress (horizontal orientation) exhibited lower fatigue life. The yield stress of vertical specimens is 16% lower than the uniaxial fatigue strength.
- Comparison of the obtained fatigue data for ER70S-6 WAAM built specimens with the existing fatigue data on structural steels in the literature revealed that the S-N data from this study overlap with the upper bound of the fatigue results for wrought S355 steel.
- The S-N fatigue data from this study exhibited a higher trend compared to the recommended DNV C1 design curve. This suggests that the tested material and WAAM technique can be considered to be used for fabrication of offshore structures.
- Analysis of the fatigue data on torsion and multiaxial fatigue available in the literature demonstrated similar trends with C40 carbon steel and S355 steel.
- Fracture surfaces of six specimens (two orientations for each fatigue load type) were analysed with SEM and fracture mechanisms and features were compared for different types of loading. The WAAM

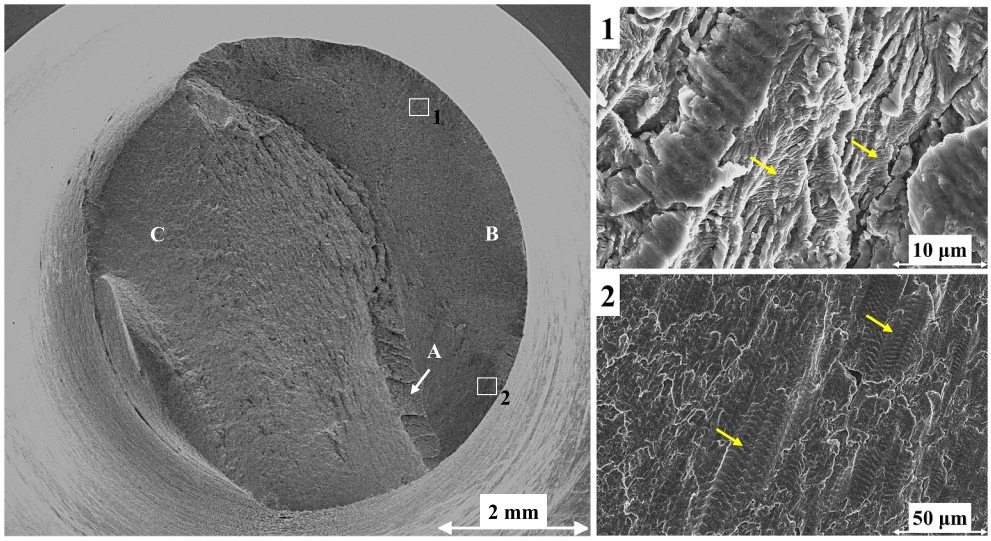

(a)

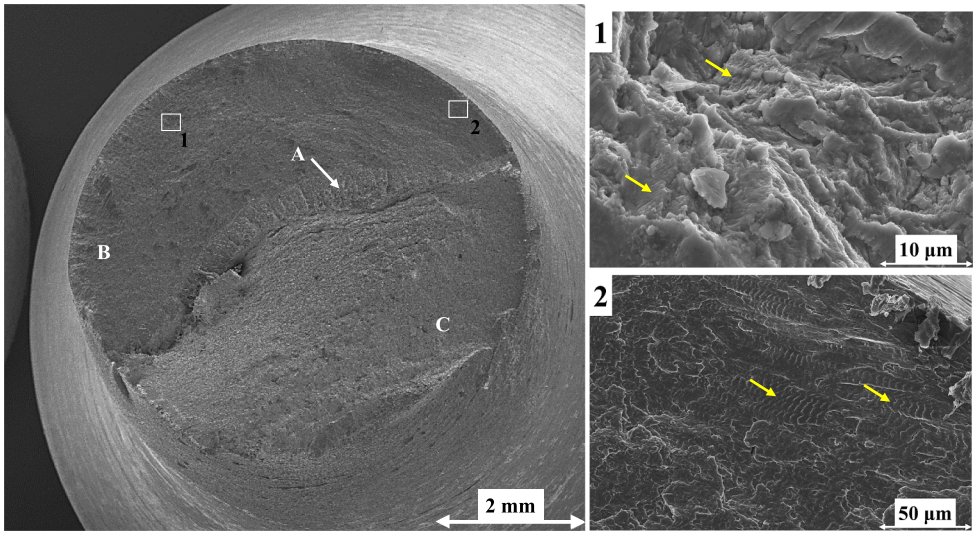

(b)

Fig. 9. Fracture surface of ER70S-6 WAAM built specimens tested under multiaxial loading condition (a) for vertical, and (b) for horizontal specimens, presenting fatigue (1) and fishbone (2) features.

built material employed in this study was found to be almost defect-free with some minor defects of smaller than 30 µm.

Declaration of Competing Interest

The authors declare that they have no known competing financial interests or personal relationships that could have appeared to influence the work reported in this paper.

Acknowledgements

This work was supported by grant EP/L016303/1 for Cranfield, Oxford and Strathclyde Universities' Centre for Doctoral Training in Renewable Energy Marine Structures – REMS CDT (http://www.remscdt.ac.uk/) from the UK Engineering and Physical Sciences Research Council (EPSRC). Special thanks to the NTNU structural integrity research group for conducting the fatigue testing in their laboratory.

References

[1] Razavi SMJ, Ferro P, Berto F. Fatigue assessment of Ti–6Al–4V circular notched specimens produced by selective laser melting. Metals (Basel) 2017;7:1–10.
[2] Fotovvati B, Namdari N, Dehghanghadikolaei A. Fatigue performance of selective laser melted Ti6Al4V components: State of the art. Mater Res Express 2019;6(1):012002.
[3] Lee YS, Zhang W. Modeling of heat transfer, fluid flow and solidification microstructure of nickel-base superalloy fabricated by laser powder bed fusion. Addit Manuf 2016;12:178–88.
[4] Domashenkov A, Plotnikova A, Movchan I, Bertrand P, Peillon N, Desplanques B, et al. Microstructure and physical properties of a Ni/Fe-based superalloy processed by Selective Laser Melting. Addit Manuf 2017;15:66–77.
[5] Todai M, Nakano T, Liu T, Yasuda HY, Hagihara K, Cho K, et al. Effect of building direction on the microstructure and tensile properties of Ti-48Al-2Cr-2Nb alloy additively manufactured by electron beam melting. Addit Manuf 2017;13:61–70.
[6] Bartsch H, Kühne R, Citarelli S, Schaffrath S, Feldmann M. Fatigue analysis of wire arc additive manufactured (3D printed) components with unmilled surface. Structures 2021;31:576–89.
[7] Seow CE, Zhang J, Coules HE, Wu G, Jones C, Ding J, et al. Effect of crack-like defects on the fracture behaviour of Wire + Arc Additively Manufactured nickel-base Alloy 718. Addit Manuf 2020;36:101578.

[8] Ermakova A, Mehmanparast A, Ganguly S. A review of present status and challenges of using additive manufacturing technology for offshore wind applications. Procedia Struct Integr 2019;17:29–36.
[9] ASM. ASM International Fatigue. *Elem. Metall. Eng. Alloy.* 243–265 (2008).
[10] Pegues J, Roach M, Scott Williamson R, Shamsaei N. Surface roughness effects on the fatigue strength of additively manufactured Ti-6Al-4V. Int J Fatigue 2018;116:543–52.
[11] Syed AK, Zhang X, Caballero A, Shamir M, Williams S. Influence of deposition strategies on tensile and fatigue properties in a wire + arc additive manufactured Ti-6Al-4V. Int J Fatigue 2021;149:106268.
[12] Springer, S., Leitner, M., Gruber, T., Oberwinkler, B., Lasnik, M. & Grün, F. Fatigue Assessment of Wire and Arc Additively Manufactured Ti-6Al-4V. *Met. 2022, Vol. 12, Page 795* **12**, 795 (2022).
[13] Biswal, R., Zhang, X., Shamir, M., Al Mamun, A., Awd, M., Walther, F. & Khadar Syed, A. Interrupted fatigue testing with periodic tomography to monitor porosity defects in wire + arc additive manufactured Ti-6Al-4V. *Addit. Manuf.* **28**, 517–527 (2019).
[14] Shamir M, Syed AK, Janik V, Biswal R, Zhang X. The role of microstructure and local crystallographic orientation near porosity defects on the high cycle fatigue life of an additive manufactured Ti-6Al-4V. Mater Charact 2020;169:110576.
[15] Shrestha R, Simsiriwong J, Shamsaei N. Fatigue behavior of additive manufactured 316L stainless steel under axial versus rotating-bending loading: synergistic effects of stress gradient, surface roughness, and volumetric defects. Int J Fatigue 2021;144:106063.
[16] Zulić S, Rostohar D, Kaufman J, Pathak S, Kopeček J, Böhm M, et al. Fatigue life enhancement of additive manufactured 316l stainless steel by LSP using a DPSS laser system. Surf Eng 2022;38(2):183–90.
[17] Dirisu P, Supriyo G, Martina F, Xu X, Williams S. Wire plus arc additive manufactured functional steel surfaces enhanced by rolling. Int J Fatigue 2020;130:105237.
[18] Lincoln Electric Company, T. *LINCOLN ® ER70S-6 WELDING POSITIONS TYPICAL APPLICATIONS*.
[19] Standard Practice for Conducting Force Controlled Constant Amplitude Axial Fatigue Tests of Metallic Materials. Available at: https://www.astm.org/e0466-21.html. (Accessed: 5th July 2022).
[20] BS ISO 12107-2003–[2022-07-06–10-12-27 AM].pdf.
[21] Testing, F. Standard Practice for Statistical Analysis of Linear or Linearized Stress-Life (. *Stat. Anal. Fatigue Data* **91**, 129-129–9 (2009).
[22] Ermakova A, Mehmanparast A, Ganguly S, Razavi J, Berto F. Investigation of mechanical and fracture properties of wire and arc additively manufactured low carbon steel components. Theor Appl Fract Mech 2020;109:102685.
[23] Anandavijayan S, Mehmanparast A, Braithwaite J, Brennan F, Chahardehi A. Material pre-straining effects on fatigue behaviour of S355 structural steel. J Constr Steel Res 2021;183:106707.
[24] (DNV) Det Norske Veritas. Fatigue Design of Offshore Steel Structures. *Recomm. Pract. DNV-RPC203* 126 (2005).
[25] Razavi SMJ, Van Hooreweder B, Berto F. Effect of build thickness and geometry on quasi-static and fatigue behavior of Ti-6Al-4V produced by Electron Beam Melting. Addit Manuf 2020;36:101426.
[26] Berto F, Campagnolo A, Lazzarin P. Fatigue strength of severely notched specimens made of Ti-6Al-4V under multiaxial loading. Fatigue Fract Eng Mater Struct 2015;38:503–17.
[27] Li P, Warner DH, Fatemi A, Phan N. Critical assessment of the fatigue performance of additively manufactured Ti-6Al-4V and perspective for future research. Int J Fatigue 2016;85:130–43.
[28] Mehmanparast A, Taylor J, Brennan F, Tavares I. Experimental investigation of mechanical and fracture properties of offshore wind monopile weldments: SLIC interlaboratory test results. Fatigue Fract Eng Mater Struct 2018;41:2485–501.
[29] Mehmanparast A, Brennan F, Tavares I. Fatigue crack growth rates for offshore wind monopile weldments in air and seawater: SLIC inter-laboratory test results. Mater Des 2017;114:494–504.
[30] Corigliano P, Cucinotta F, Guglielmino E, Risitano G, Santonocito D. Fatigue assessment of a marine structural steel and comparison with Thermographic Method and Static Thermographic Method. Fatigue Fract Eng Mater Struct 2020;43:734–43.
[31] Dantas R, Correia J, Lesiuk G, Rozumek D, Zhu SP, de Jesus A, et al. Evaluation of multiaxial high-cycle fatigue criteria under proportional loading for S355 steel. Eng Fail Anal 2021;120:105037.
[32] Aeran A, Acosta R, Siriwardane SC, Starke P, Mikkelsen O, Langen I, et al. A nonlinear fatigue damage model: Comparison with experimental damage evolution of S355 (SAE 1020) structural steel and application to offshore jacket structures. Int J Fatigue 2020;135:105568.
[33] Berto F, Mutignani F, Pittarello L. Effect of hot-dip galvanization on the fatigue behaviour of welded structural steel. Procedia Struct Integr 2016;2:1813–20.
[34] Atzori B, Berto F, Lazzarin P, Quaresimin M. Multi-axial fatigue behaviour of a severely notched carbon steel. Int J Fatigue 2006;28(5-6):485–93.
[35] Berto F, Lazzarin P, Yates JR. Multiaxial fatigue of V-notched steel specimens: a non-conventional application of the local energy method. Fatigue Fract Eng Mater Struct 2011;34:921–43.
[36] Berto F, Lazzarin P, Marangon C. Fatigue strength of notched specimens made of 40CrMoV13.9 under multiaxial loading. Mater Des 2014;54:57–66.